

## Lock-in spin structures and ferrimagnetism in polar $\text{Ni}_{2-x}\text{Co}_x\text{ScSbO}_6$ oxides

Kun-lang Ji,<sup>a</sup> Elena Solana-Madruga,<sup>a</sup> Angel M. Arevalo-Lopez,<sup>b</sup> Pascal Manuel,<sup>c</sup> Clemens Ritter,<sup>d</sup> Anatoliy Senyshyn<sup>e</sup> and J. Paul Attfield\*<sup>a</sup>

### Supplementary Experimental Details:

#### **Synthesis**

$\text{Ni}_{2-x}\text{Co}_x\text{ScSbO}_6$  ( $x = 0, 0.5, 1$  and  $1.5$ ) have been prepared by conventional solid-state synthesis. The precursor mixtures were prepared by grinding together the stoichiometric proportions of binary oxides NiO, CoO,  $\text{Sc}_2\text{O}_3$  and  $\text{Sb}_2\text{O}_5$  under acetone. Previous heat treatments were used for NiO and CoO to ensure their stoichiometry. The precursors were then pelletized and heated at increasing temperatures between 973 K and 1373 K for 24 hours in steps of 100 K with intermediate grinding and repelletizing. The attempted synthesis of the  $x = 2$  compound following this approach was found to lead to large amounts of secondary phase  $\text{Co}_{2.33}\text{Sb}_{0.64}\text{O}_4$  spinel. Pure  $\text{Co}_2\text{ScSbO}_6$  has consequently been synthesized under high pressure-high temperature (HPHT) conditions using a multi-anvil apparatus. The precursor, also prepared from the stoichiometric CoO,  $\text{Sc}_2\text{O}_3$  and  $\text{Sb}_2\text{O}_5$  oxides, was packed into a Pt capsule and assembled into a Walker module. The synthesis conditions were 6 GPa with heating at 1273 K for one hour followed by slow cooling and then decompression.

#### **Powder X-ray diffraction**

Laboratory powder XRD data were collected for  $\text{Ni}_{2-x}\text{Co}_x\text{ScSbO}_6$  at room temperature in the  $10^\circ < 2\theta < 70^\circ$  angular range with a  $0.03^\circ$  step size and counting time 0.45s per step, using a  $\lambda = 1.54050 \text{ \AA}$  copper  $K\alpha$  radiation source on a D2 Bruker x-ray diffractometer. The ordered NTO-type structural model was refined by fitting the X-ray data using the GSAS software package<sup>1-2</sup>. The resulting fits are depicted in Figure SF1. For these refinements, the background was modelled with a polynomial function (Shifted Chebyshev) and the peak shape was fitted using a pseudo-Voigt function. XRD patterns reveal that the target phase  $\text{Ni}_{2-x}\text{Co}_x\text{ScSbO}_6$  formed predominantly along with (Co,Ni)O and  $\text{Sc}_{5.5}\text{Sb}_{1.5}\text{O}_{12}$  secondary phases for  $x = 0, 0.5$  and  $2$ , and additional  $\text{Co}_{2.33}\text{Sb}_{0.64}\text{O}_4$  spinel for  $x = 1$  and  $1.5$  compounds. The sample colour varies from green ( $x = 0$ ) to dark red ( $x = 0.5$ ) and finally to purple ( $x = 2$ ) as depicted in Figure SF1 insets. The dark purple colours of intermediate compositions  $x = 1$  and  $1.5$  are due to the black secondary  $\text{Co}_{2.33}\text{Sb}_{0.64}\text{O}_4$  oxide.

#### **Powder neutron diffraction**

##### Experimental details

Low temperature neutron powder diffraction (NPD) profiles were collected from samples in sealed vanadium cans within He cryostats at several facilities;

- For  $\text{Ni}_{2-x}\text{Co}_x\text{ScSbO}_6$  ( $x = 0, 0.5, 1$  and  $1.5$ ) data at 4, 30, 50, 70 and 100 K were collected using the SPODI beamline of FRMII (Munich, Germany). The diffraction data were collected over the range  $0^\circ < 2\theta < 150^\circ$  with a constant neutron wavelength  $\lambda = 1.538 \text{ \AA}$  for  $x = 0$  and  $\lambda = 2.536 \text{ \AA}$  for  $x \neq 0$  and a step-width of  $0.05^\circ$ .
- Further NPD data for  $x = 1.5$  were collected at D20 instrument of the Institut Laue-Langevin (Grenoble, France) at 1.5 and 70 K using a similar wavelength  $\lambda = 2.41 \text{ \AA}$  and at 25, 50 and 70 K using a longer wavelength  $\lambda = 3.594 \text{ \AA}$ . As detailed below, the latter measurements allowed the resolution of two coexisting magnetic phases being ordered at the same transition temperature with similar  $[0\ 0\ 0]$  and  $[0\ 0\ k_z]$  propagation vectors for small  $k_z$ . A new monochromator, recently custom built for D20 to select this long wavelength, was used for the first time to measure this sample using the high take off angle mode. This proved a powerful tool for studying long-period magnetic orders.
- NPD data of 50mg of the HPHT  $\text{Co}_2\text{ScSbO}_6$  sample were collected at the high-resolution TOF WISH diffractometer at ISIS facility (Oxford, U.K.) at 1.7, 10, 20, 30, 40, 55, 60, 70 and 100 K.

In all cases the 100 K data, well above the magnetic transition temperatures  $T_C \sim 60$  K, were fit with the Rietveld method to refine the structural models using the FullProf software package<sup>3</sup> and a pseudo-Voigt profile function to describe the shape of the diffraction peaks. The background was fitted using equidistant experimental points and modelled using an interpolation method. The patterns could be fit using the NTO structure determined from the initial fits of the XRD patterns as a starting model. The resulting structural features, including accurate atomic positions, relative occupancies, thermal factors and BVS calculations are summarized in Tables ST1 – ST5. The Rietveld fits are shown in Figure SF2 and the evolution of the lattice parameters is depicted in Figure SF3. The main interatomic distances and angles arising from these refinements are summarized in Table ST6, where the octahedral distortions ( $\Delta$ ) have also been calculated as indicated in the Table caption. The low temperature NPD data were used to determine the magnetic structures of  $\text{Ni}_{2-x}\text{Co}_x\text{ScSbO}_6$ . As described in the main text, magnetic satellite reflections were indexed by  $[0\ k_y\ 0]^4$  and  $[0\ 0\ k_z]$  vectors for  $x = 0$  and  $x \neq 0$  respectively. An additional contribution on top of the nuclear Bragg (003) peak appears in  $x = 1.5$  and  $x = 2$  compounds, revealing an additional commensurate magnetic phase with propagation vector  $k = [0\ 0\ 0]$ . The commensurate magnetic contribution is clearly observed for the complete temperature range below  $T_C$  for  $x = 2$  WISH data. However, it is not clearly resolved for  $x = 1.5$  compound from the SPODI data as shown on the right panel of Figure SF8, which shows the 50 K – 70 K and 4 K – 70 K difference patterns. The left panel of the figure shows similar difference patterns collected at D20 with the longer wavelength  $\lambda = 3.594$  Å. The longer wavelength yields a better resolution of the satellite peaks, which allows the observation of the commensurate magnetic contribution just below  $T_C$ .

#### Magnetic symmetry analysis

The magnetic symmetry analysis (Table ST7) of the low temperature NPD data was performed by means of Baslreps<sup>5</sup> software. The irreducible representations (Irep) and basis vectors (BV) resulting for the incommensurate propagations vector  $[0\ 0\ k_z]$  is summarized in the table. Their BVs describe alignment of the spins parallel to the  $z$  axis ( $\psi_1$ ) or in planes of clockwise (CW,  $\psi_2$ ) or counterclockwise (CCW,  $\psi_3$ ) spirals. All the Rietveld fits of the low temperature NPD data (Figure SF6) have been performed using Irep  $\Gamma_2$  for the incommensurate magnetic structures although powder diffraction does not distinguish between CW and CCW helices, so  $\Gamma_3$  would be equally applicable. The commensurate  $[0\ 0\ 0]$  component has another three possible Ireps as shown in the bottom row of the table, which allow the orientation of the spins along the  $z$  axis ( $\psi_1$ ) or confined to the  $xy$  plane with independent FM ( $\psi_2$ ) or AFM ( $\psi_3$ ) components. The intensities were fitted using Irep  $\Gamma_2$  with spins confined along the  $x$  axis.

#### **Magnetization**

Zero Field Cooling (ZFC) and Field Cooling (FC) magnetic susceptibility measurements were performed on a Quantum Design MPMS-SQUID magnetometer and a Quantum Design PPMS system in the temperature range  $2\text{ K} < T < 300\text{ K}$  under a magnetic field of 1T. Magnetization measurements as a function of the applied magnetic field were measured at 2, 40 and 100 K at magnetic fields up to 5 T. Figure SF4 shows the results of the ZFC-FC data for all the compounds including reciprocal susceptibilities and their Curie-Weiss fits. Figure SF5 shows the field dependent magnetization loops of each compound. The extrapolated spontaneous magnetizations ( $M_s$ ) and critical fields ( $H_c$ ) for the metamagnetic transitions are labelled. The inset in the  $x = 1$  plot shows the enlarged region of the loop where the metamagnetic transition is observed.

Supplementary Figures:

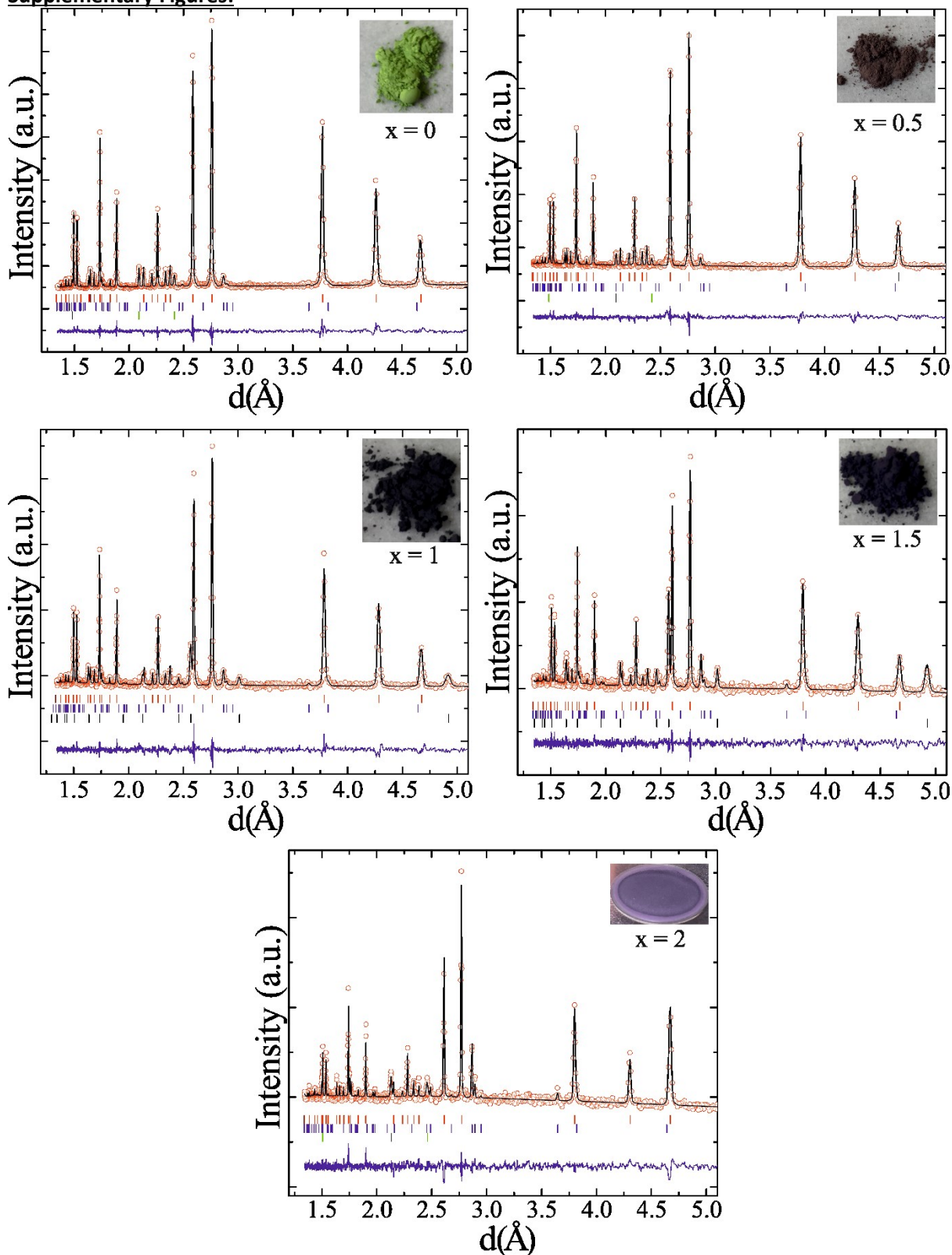


**Figure SF1.** Rietveld fits of the room temperature XRD patterns of the NTO  $\text{Ni}_{2-x}\text{Co}_x\text{ScSbO}_6$  compounds. The secondary  $\text{Sc}_{5.5}\text{Sb}_{1.5}\text{O}_{12}$  (blue) and  $(\text{Ni}/\text{Co})\text{O}$  phases (green) are included in all the refinements and the additional  $\text{Co}_{2.33}\text{Sb}_{0.64}\text{O}_4$  spinel (black) is included for  $x = 1$  and  $1.5$ . The inset photos show the sample colours.

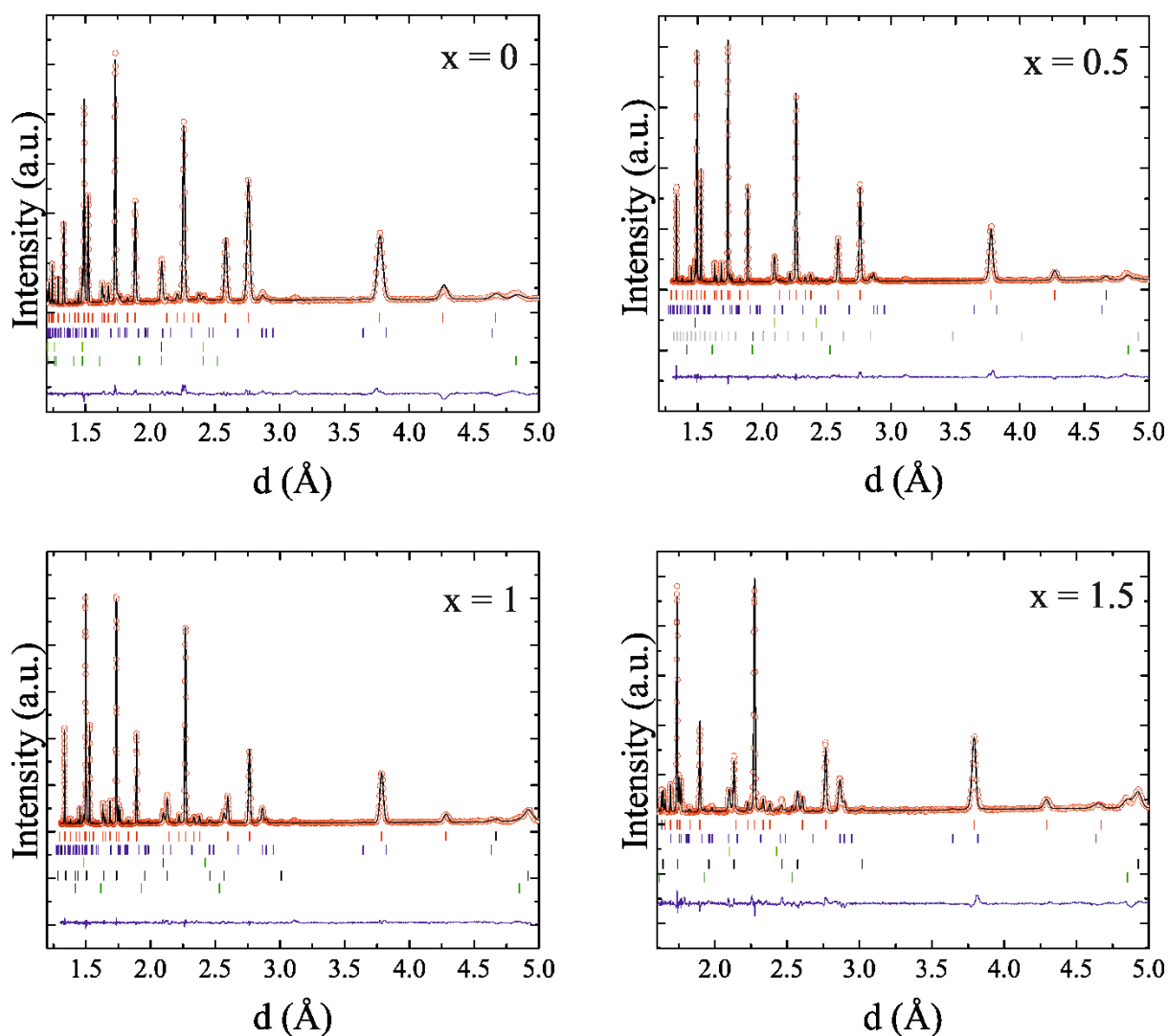


**Figure SF2.** Rietveld fits of the NPD patterns of the NTO  $\text{Ni}_{2-x}\text{Co}_x\text{ScSbO}_6$  compounds collected at 100 K. The secondary  $\text{Sc}_{5.5}\text{Sb}_{1.5}\text{O}_{12}$  (blue) is included in all refinements (5.7, 6.9, 10.0 and 16.6 %). Nuclear (green) and magnetic structures (olive) of the (Ni/Co)O phases are also included in the refinements (4.1, 5.9, 2.5 and 3.0 %). The additional  $\text{Co}_{2.33}\text{Sb}_{0.64}\text{O}_4$  spinel (black) is included for  $x = 1, 1.5$  (16.4 and 15.0 %) and  $\text{Sc}_2\text{O}_3$  (grey) is included in  $x = 0.5$  (1%).

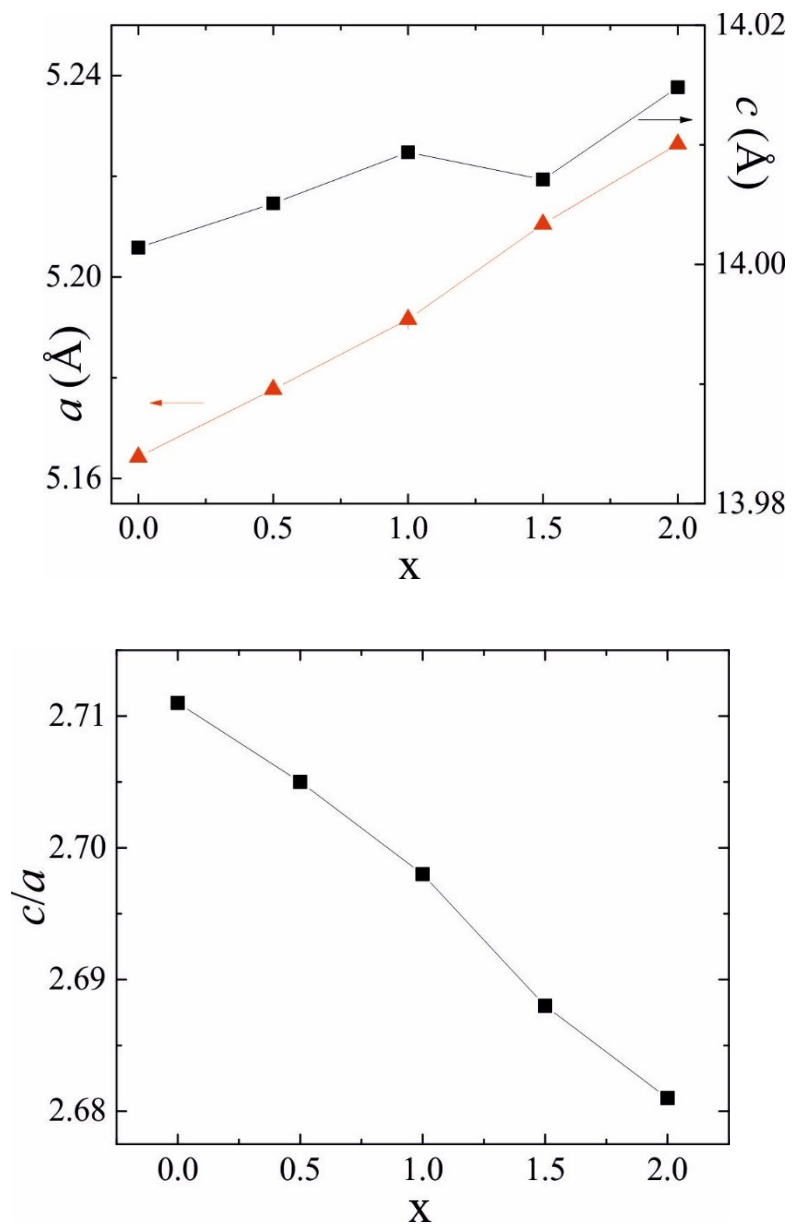


**Figure SF3.** Evolution of the lattice parameters (top) and the  $c/a$  ratio (bottom) of  $\text{Ni}_{2-x}\text{Co}_x\text{ScSbO}_6$  as a function of the chemical composition, showing that the solid solutions have been formed and exhibit structural anisotropy resulting from the electronic degeneracy of the  $\text{Co}^{2+}$  ions

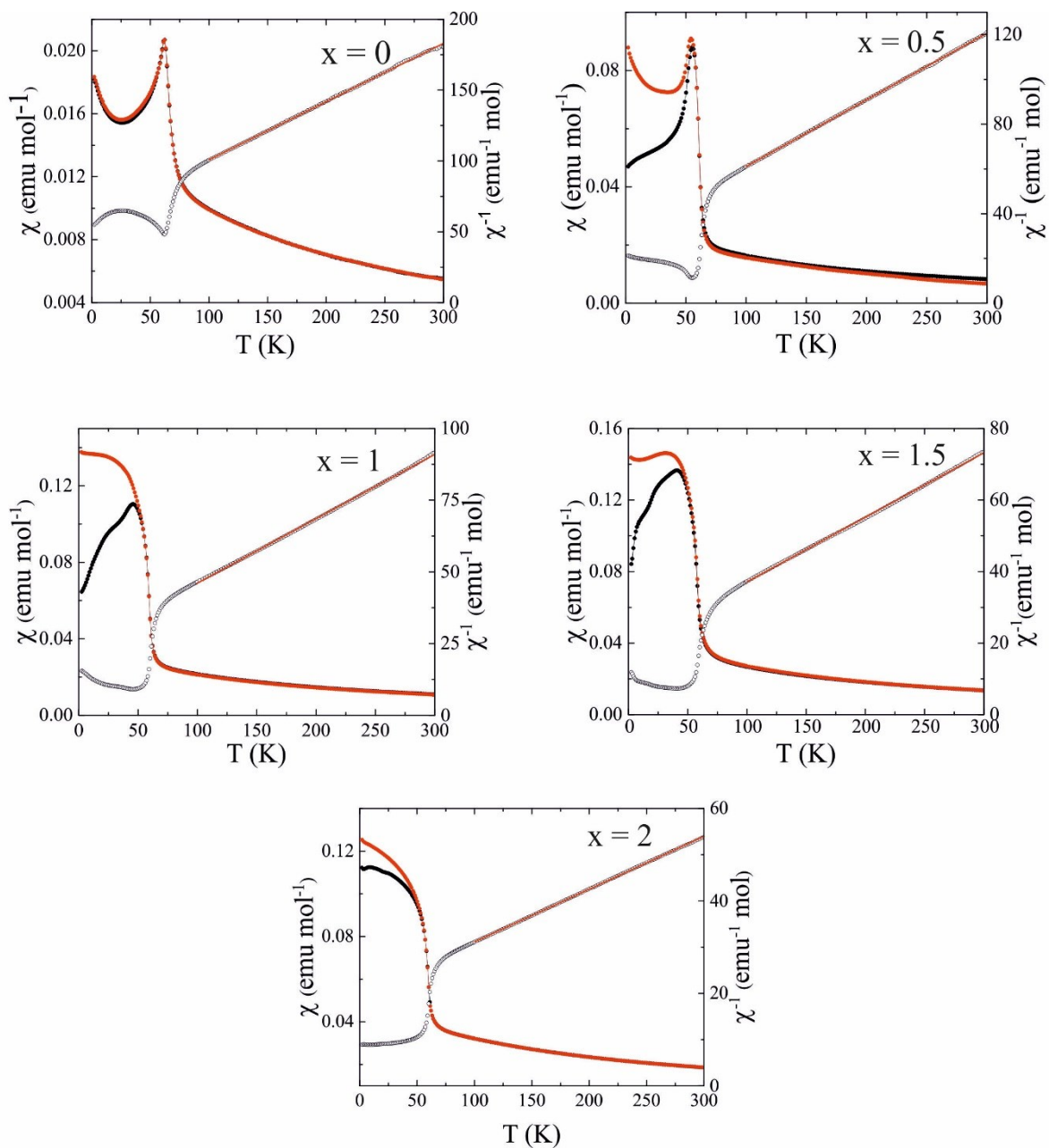


**Figure SF4.** ZFC-FC magnetic susceptibility of  $\text{Ni}_{2-x}\text{Co}_x\text{ScSbO}_6$  as a function of temperature under an applied magnetic field of 1 T (black and red circles). Reciprocal susceptibility (open circles) is on the right axis and fitted (red line) to the Curie–Weiss law.

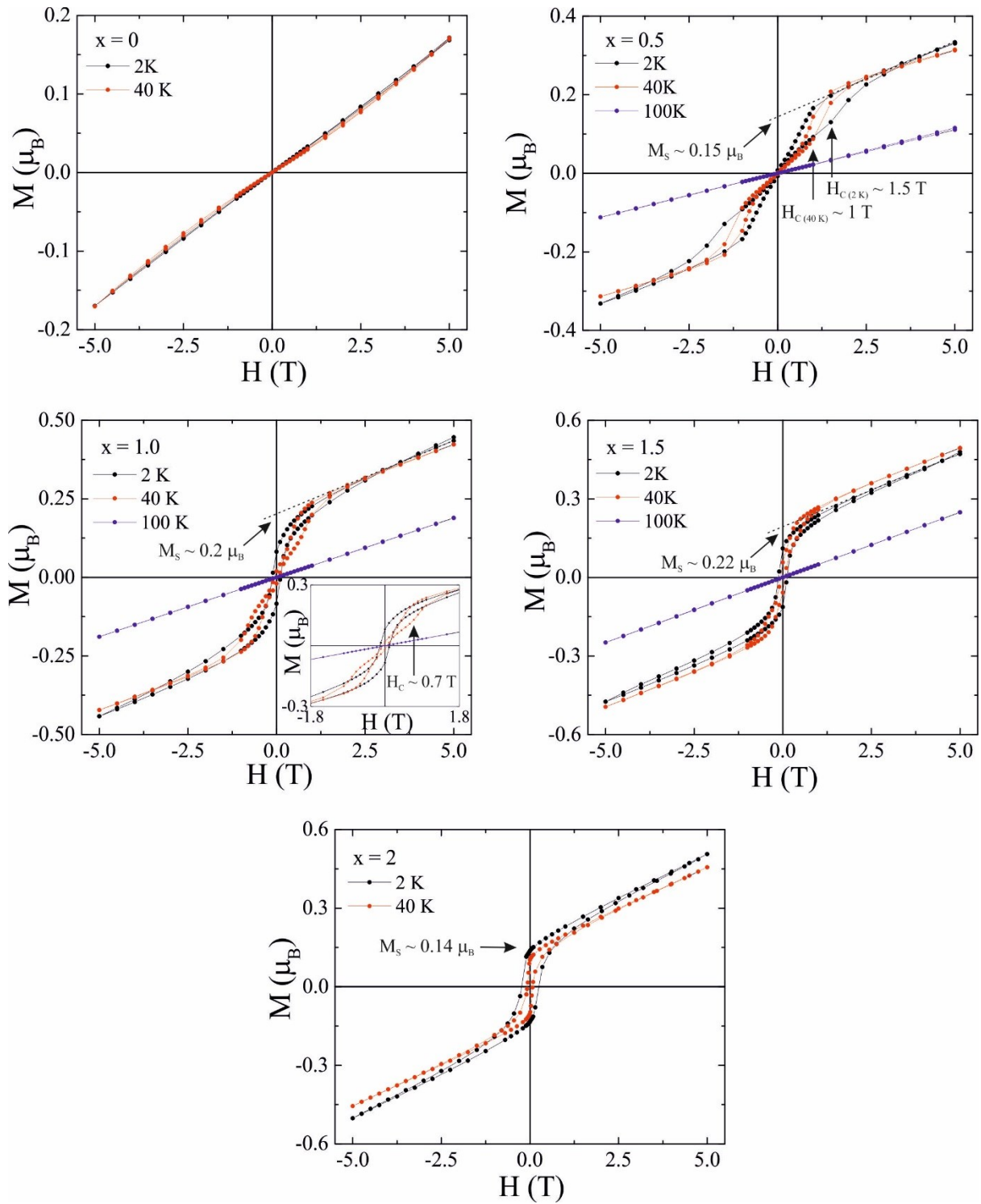


**Figure SF5.** Field dependent magnetization loops of  $\text{Ni}_{2-x}\text{Co}_x\text{ScSbO}_6$  at different temperatures. Spontaneous magnetizations ( $M_s$ ) and critical fields ( $H_c$ ) are labelled. The inset in  $x = 1$  plot shows an enlargement of the metamagnetic transitions.

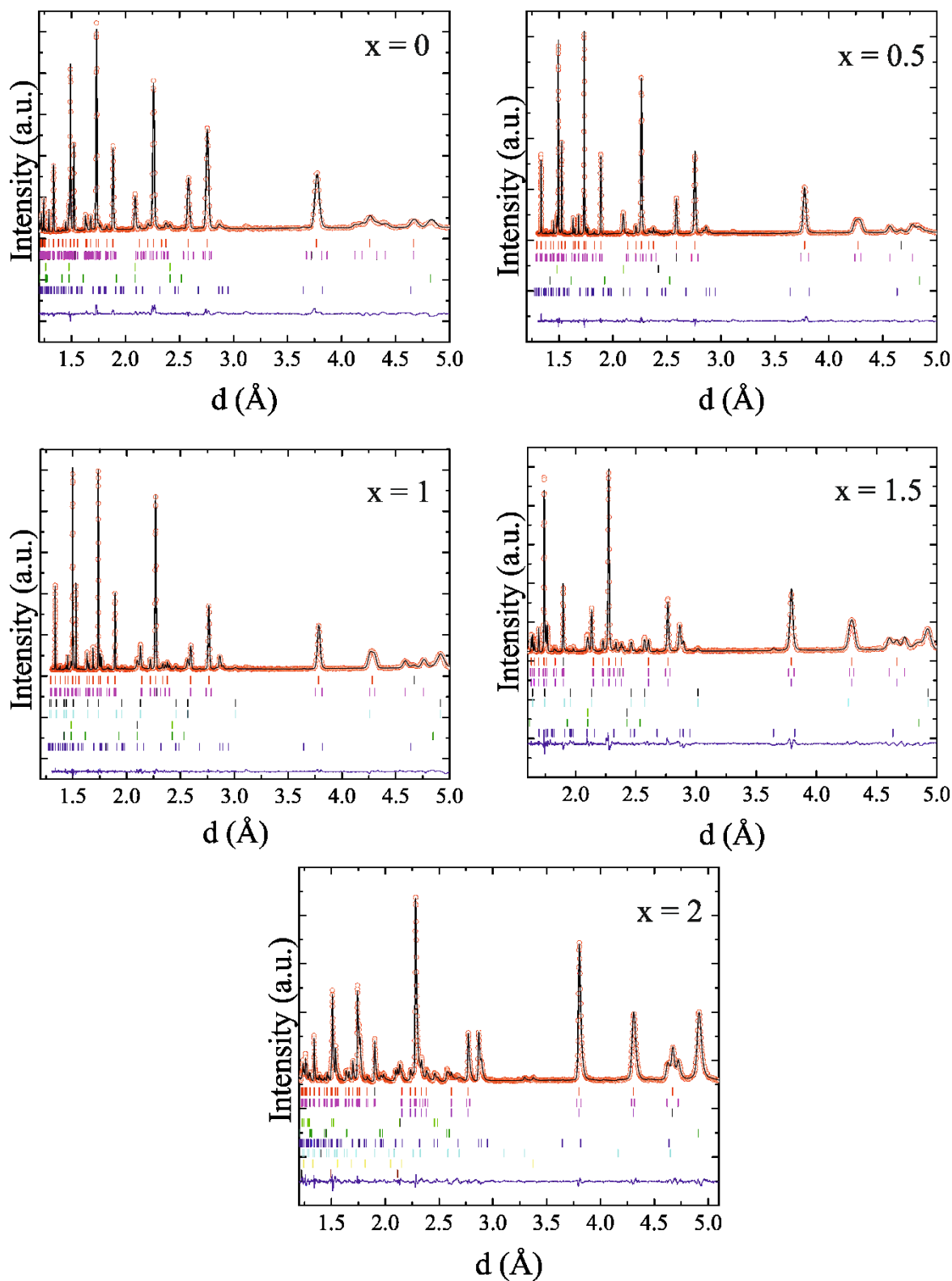


**Figure SF6.** Rietveld fits of the NPD patterns of the NTO  $\text{Ni}_{2-x}\text{Co}_x\text{ScSbO}_6$  compounds collected at 4 K and  $\text{Co}_2\text{ScSbO}_6$  NPD data collected at 1.7 K. The secondary  $\text{Sc}_{5.5}\text{Sb}_{1.5}\text{O}_{12}$  (blue) and nuclear (green) and magnetic structures (olive) of the (Ni/Co)O phases are included in all refinements. The nuclear (black) and magnetic structure (light blue) of  $\text{Co}_{2.33}\text{Sb}_{0.64}\text{O}_4$  spinel phases are included for  $x = 1, 1.5$ . The cyan, yellow and dark red tick marks refer to secondary scattering from  $\text{CoSb}_2\text{O}_6$ , BN and V respectively in high-pressure phase  $x = 2$ .

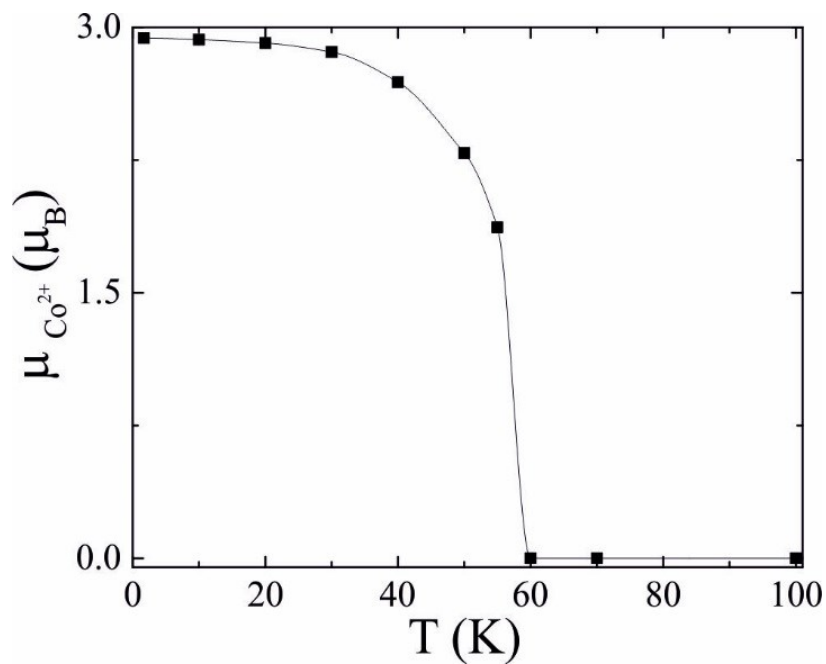


**Figure SF7.** Thermal evolution of the magnetic moments of  $\text{Co}_2\text{ScSbO}_6$  from the Rietveld fits of the NPD data collected at WISH at different temperatures.

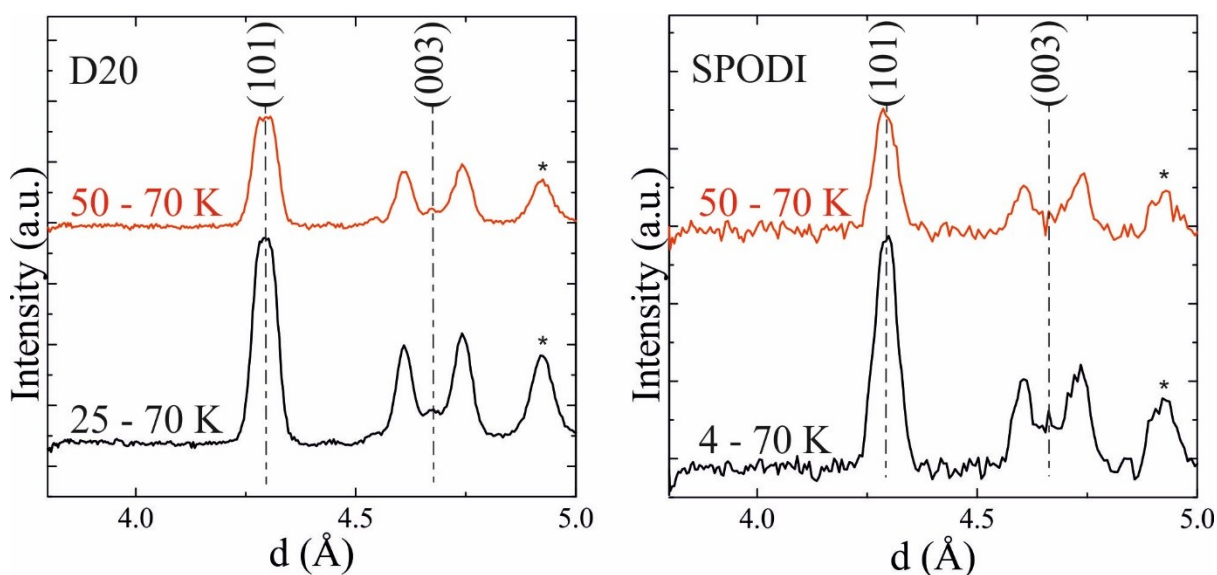


**Figure SF8.** 50 K – 70 K (red), 25 K – 70 K and 4 K – 70 K (black) NPD difference patterns of  $\text{Ni}_{0.5}\text{Co}_{1.5}\text{ScSbO}_6$  collected at D20 (left) and SPODI (right). (003) and (101) main magnetic peaks are labelled and identified with dashed lines. Secondary  $\text{Co}_{2.33}\text{Sb}_{0.64}\text{O}_4$  magnetic signal is identified with an asterisk.

### Supplementary tables:

**Table ST1.** Crystallographic details of the NTO-type structure of  $\text{Co}_2\text{ScSbO}_6$  from the Rietveld fit of 100 K NPD pattern, using space group  $R3$  and cell parameters  $a = 5.2264(1)$  Å and  $c = 14.0148(4)$  Å. BVS and cationic displacements ( $d$ ) in the puckered (00l) layers, calculated from these results, are included in the two last columns.

Wyckoff	Atom	x	y	z	Occ	$B_{\text{iso}}(\text{Å}^2)$	BVS	$d(\text{Å})$
3a	Co1	1/3	2/3	0.150(2)	1.0	0.6(1)	1.64	0.234
3a	Co2/Sc	2/3	1/3	0.300(2)	0.951/0.048(3)	0.6(1)	2.12	0.467
3a	Sc/Co2	2/3	1/3	0.515(1)	0.792/0.207(3)	0.6(1)	2.93	-0.210
3a	Sb	1/3	2/3	0.350(1)	1.0	0.6(1)	5.66	-0.234
9b	O1	0.323(1)	0.035(2)	0.072(1)	1.0	0.88(1)	–	–
9b	O2	0.323(1)	0.360(1)	1/4	1.0	0.88(1)	–	–

$R_p=2.49\%$ ,  $R_{wp}=3.06\%$ ,  $R_B=3.71\%$ ,  $R_F=5.50\%$ .

**Table ST2.** Crystallographic details of the NTO-type structure of  $\text{Ni}_2\text{ScSbO}_6$  from the Rietveld fit of 100 K NPD pattern, using space group  $R3$  and cell parameters  $a = 5.16427(2)$  Å and  $c = 14.0014(1)$  Å. BVS and cationic displacements ( $d$ ) in the puckered (00l) layers, calculated from these results, are included in the two last columns.

Wyckoff	Atom	x	y	z	Occ	$B_{\text{iso}}(\text{Å}^2)$	BVS	$d(\text{Å})$
3a	Ni1	1/3	2/3	0.1437(4)	1.0	0.78(1)	1.80	0.322
3a	Ni2	2/3	1/3	0.3145(4)	1.0	0.78(1)	1.94	0.264
3a	Sc	2/3	1/3	0.5168(6)	1.0	0.78(1)	3.17	-0.235
3a	Sb	1/3	2/3	0.348(1)	1.0	0.78(1)	5.01	-0.205
9b	O1	0.316(1)	0.016(1)	0.0796(4)	1.0	0.85(1)	–	–
9b	O2	0.329(2)	0.364(1)	1/4	1.0	0.85(1)	–	–

$R_p=3.43\%$ ,  $R_{wp}=4.31\%$ ,  $R_B=3.34\%$ ,  $R_F=1.90\%$ .

**Table ST3.** Crystallographic details of the NTO-type structure of  $\text{Ni}_{1.5}\text{Co}_{0.5}\text{ScSbO}_6$  from the Rietveld fit of 100 K NPD pattern, using space group  $R3$  and cell parameters  $a = 5.17768(3)$  Å and  $c = 14.0051(1)$  Å. BVS and cationic displacements ( $d$ ) in the puckered (00l) layers, calculated from these results, are included in the two last columns.

Wyckoff	Atom	x	y	z	Occ	$B_{\text{iso}}(\text{Å}^2)$	BVS	$d(\text{Å})$
3a	M1 (Ni/Co)	1/3	2/3	0.1494(3)	0.712/0.288(3)	0.3(1)	1.82	0.241
3a	M2 (Ni/Co)	2/3	1/3	0.3196(4)	0.79/0.21(1)	0.3(1)	1.82	0.192
3a	Sc/Co2	2/3	1/3	0.5246(3)	0.928/0.072(3)	0.3(1)	3.15	-0.344
3a	Sb	1/3	2/3	0.3506(4)	1.0	0.3(1)	5.31	-0.242
9b	O1	0.323(1)	0.023(1)	0.079(1)	1.0	0.4(1)	–	–
9b	O2	0.325(1)	0.366(1)	1/4	1.0	0.4(1)	–	–

$R_p=3.80\%$ ,  $R_{wp}=5.05\%$ ,  $R_B=3.00\%$ ,  $R_F=2.20\%$ .

**Table ST4.** Crystallographic details of the NTO-type structure of NiCoScSbO<sub>6</sub> from the Rietveld fit of 100 K NPD pattern, using space group *R3* and cell parameters *a* = 5.19158 (1) Å and *c* = 14.00937 (5) Å. BVS and cationic displacements (*d*) in the puckered (00*l*) layers, calculated from these results, are included in the two last columns.

Wyckoff	Atom	x	y	z	Occ	B <sub>iso</sub> (Å <sup>2</sup> )	BVS	d(Å)
3a	M1 (Ni/Co)	1/3	2/3	0.1409(4)	0.482/0.518(3)	0.59(5)	1.79	0.361
3a	M2 (Ni/Co)	2/3	1/3	0.3174(3)	0.652/0.348(5)	0.59(5)	1.81	0.223
3a	Sc/Co2	2/3	1/3	0.5193(3)	0.829/0.171(3)	0.59(5)	3.12	-0.270
3a	Sb	1/3	2/3	0.3485(4)	1.0	0.59(5)	4.91	-0.212
9b	O1	0.321(1)	0.024(1)	0.085(1)	1.0	0.4(1)	–	–
9b	O2	0.335(1)	0.371(1)	1/4	1.0	0.4(1)	–	–

$R_p=3.26\%$ ,  $R_{wp}=4.48\%$ ,  $R_B=1.08\%$ ,  $R_F=1.10\%$ .

**Table ST5.** Crystallographic details of the NTO-type structure of Ni<sub>0.5</sub>Co<sub>1.5</sub>ScSbO<sub>6</sub> from the Rietveld fit of 100 K NPD pattern, using space group *R3* and cell parameters *a* = 5.21051 (2) Å and *c* = 14.0071 (1) Å. BVS and cationic displacements (*d*) in the puckered (00*l*) layers, calculated from these results, are included in the two last columns.

Wyckoff	Atom	x	y	z	Occ	B <sub>iso</sub> (Å <sup>2</sup> )	BVS	d(Å)
3a	M1 (Ni/Co)	1/3	2/3	0.142(2)	0.184/0.816(5)	0.4(1)	1.65	0.345
3a	M2 (Ni/Co)	2/3	1/3	0.306(1)	0.343/0.657(6)	0.4(1)	1.84	0.383
3a	Sc/Co2	2/3	1/3	0.514(1)	0.820/0.180(4)	0.4(1)	3.10	-0.196
3a	Sb	1/3	2/3	0.348(2)	1.0	0.4(1)	5.06	-0.205
9b	O1	0.321(1)	0.031(2)	0.083(1)	1.0	0.5(1)	–	–
9b	O2	0.335(2)	0.370(1)	1/4	1.0	0.5(1)	–	–

$R_p=5.90\%$ ,  $R_{wp}=7.69\%$ ,  $R_B=3.62\%$ ,  $R_F=2.05\%$ .

**Table ST6.** Bond lengths ( $d_{M-O}$ ), average M-O distances ( $d_{AV}$ ), angles and octahedral distortions ( $\Delta$ ) of  $Ni_{2-x}Co_xScSbO_6$  compounds.  $\Delta$  calculated from  $1/n \cdot \Sigma[(d-d_{AV})/d_{AV}]^2$

X	$d_{M1-O}$ (Å)	$d_{M2-O}$ (Å)	$d_{Sc-O}$ (Å)	$d_{Sb-O}$ (Å)	$\langle M1-O1-M2 \rangle^\circ$	$\langle M1-O2-M2 \rangle^\circ$
0	3 x 2.06(1)	3 x 2.11(1)	3 x 2.16(1)	3 x 1.96 (1)	128.6(2)	131.7(2)
	3 x 2.15(1)	3 x 2.04(1)	3 x 2.03(1)	3 x 2.07 (1)		
	$d_{AV} = 2.105$ (1)	$d_{AV} = 2.075$ (1)	$d_{AV} = 2.095$ (1)	$d_{AV} = 2.015$ (1)		
	$\Delta = 4.57E-4$	$\Delta = 2.85E-4$	$\Delta = 9.63E-4$	$\Delta = 7.45E-4$		
0.5	3 x 2.10(1)	3 x 2.08(1)	3 x 2.25(1)	3 x 1.91(1)	127.7(2)	131.9(3)
	3 x 2.08(1)	3 x 2.10(1)	3 x 1.97(1)	3 x 2.08(1)		
	$d_{AV} = 2.09$ (1)	$d_{AV} = 2.09$ (1)	$d_{AV} = 2.11$ (1)	$d_{AV} = 1.995$ (1)		
	$\Delta = 2.29E-5$	$\Delta = 2.29E-5$	$\Delta = 4.40E-3$	$\Delta = 1.82E-3$		
1.0	3 x 2.04(1)	3 x 2.14(1)	3 x 2.14(1)	3 x 1.97(1)	125.3(3)	133.7(3)
	3 x 2.17(1)	3 x 2.06(1)	3 x 2.05(1)	3 x 2.07(1)		
	$d_{AV} = 2.105$ (1)	$d_{AV} = 2.10$ (1)	$d_{AV} = 2.095$ (1)	$d_{AV} = 2.02$ (1)		
	$\Delta = 9.54E-4$	$\Delta = 3.63E-4$	$\Delta = 4.61E-4$	$\Delta = 6.13E-4$		
1.5	3 x 2.10(1)	3 x 2.23(2)	3 x 2.10(1)	3 x 1.95(1)	124.7(3)	130.9(3)
	3 x 2.16(2)	3 x 1.99(1)	3x 2.08(1)	3 x 2.07(2)		
	$d_{AV} = 2.13$ (2)	$d_{AV} = 2.11$ (2)	$d_{AV} = 2.09$ (1)	$d_{AV} = 2.01$ (2)		
	$\Delta = 1.98E-4$	$\Delta = 3.23E-3$	$\Delta = 2.29E-5$	$\Delta = 8.91E-4$		
2.0	3 x 2.24(2)	3 x 2.18(3)	3 x 2.22(1)	3 x 1.86(1)	127.6(3)	127.1(4)
	3 x 2.1(1)	3 x 1.99(1)	3 x 2.03(1)	3 x 2.11(1)		
	$d_{AV} = 2.17$ (2)	$d_{AV} = 2.085$ (3)	$d_{AV} = 2.125$ (1)	$d_{AV} = 1.985$ (1)		
	$\Delta = 1.04E-3$	$\Delta = 2.08E-3$	$\Delta = 1.99E-3$	$\Delta = 4.07E-3$		

**Table ST7.** Irreducible representations (Irep) and basis vectors (BV) for the magnetic symmetry analysis of  $Ni_{2-x}Co_xScSbO_6$  with propagation vectors  $[0\ 0\ k_z]$  and  $[0\ 0\ 0]$ . Both independent magnetic cation sites M1 and M2 follow the same Ireps. Irep  $\Gamma_2$  was used to refine the magnetic structures for both propagation vectors. Note that  $\Gamma_2$  and  $\Gamma_3$  Ireps of the first structure describe clockwise and counter-clockwise helices which cannot be distinguished from powder diffraction data. The  $[0\ k_y\ 0]$  structure has been refined using the Irep suggested in ref 4.

Irep (BV)	$\Gamma_1(\psi_1)$			$\Gamma_2(\psi_2)$			$\Gamma_3(\psi_3)$		
	$m_x$	$m_y$	$m_z$	$m_x$	$m_y$	$m_z$	$m_x$	$m_y$	$m_z$
$[0\ 0\ k_z]$	0	0	1	$3/2 - i\sqrt{3}/2$	$-i\sqrt{3}$	0	$3/2 + i\sqrt{3}/2$	$i\sqrt{3}$	0
$[0\ 0\ 0]$	0	0	1	1	1	0	1	-1	0

<sup>1</sup> A.C. Larson and R.B. Von Dreele, Los Alamos National Laboratory Report LAUR, 2000, 86

<sup>2</sup> B. H. Toby, *EXPGUI*, a graphical user interface for *GSAS*, *J. Appl. Cryst.*, 2000, **34**, 210

<sup>3</sup> J. Rodriguez-Carvajal, *Physica B*, 1993, **192**, 55.

<sup>4</sup> S.A. Ivanov, R. Mathieu, P. Nordblad, R. Tellgren, C. Ritter, E. Politova, G. Kaleva, A. Mosunov, S. Stefanovich and M. Weil, *Chem. Mater.*, 2013, **25**, 935.

<sup>5</sup> Rodriguez-Carvajal 2007 BASIREPS: a program for calculating irreducible representations of space groups and basis functions for axial and polar vector properties; C. Ritter, *Solid State Phenom.* 2011, **170**, 263